ELSEVIER

Astroparticle Physics 16 (2001) 1–11

Astroparticle Physics

www.elsevier.com/locate/astropart

A measurement of the average longitudinal development profile of cosmic ray air showers between 10^{17} and 10^{18} eV

T. Abu-Zayyad [a,*], K. Belov [a], D.J. Bird [b], J. Boyer [c], Z. Cao [a], M. Catanese [d], G.F. Chen [a], R.W. Clay [e], C.E. Covault [f], H.Y. Dai [a], B.R. Dawson [e], J.W. Elbert [a], B.E. Fick [f], L.F. Fortson [f,g], J.W. Fowler [f], K.G. Gibbs [f], M.A.K. Glasmacher [h], K.D. Green [f], Y. Ho [i], A. Huang [a], C.C. Jui [a], M.J. Kidd [j], D.B. Kieda [a], B.C. Knapp [c], S. Ko [a], C.G. Larsen [a], W. Lee [i], E.C. Loh [a], E.J. Mannel [c], J. Matthews [k,l], J.N. Matthews [a], B.J. Newport [f], D.F. Nitz [m], R.A. Ong [f], K.M. Simpson [e], J.D. Smith [a], D. Sinclair [h], P. Sokolsky [a], C. Song [c], J.K.K. Tang [a], S.B. Thomas [a], J.C. van der Velde [h], L.R. Wiencke [a], C.R. Wilkinson [e], S. Yoshida [a], X.Z. Zhang [i]

[a] *High Energy Astrophysics Institute, University of Utah, Salt Lake City, UT 8 4112, USA*
[b] *Defence Science and Technology Organisation, P.O. Box 1500, Salisbury, SA 5108, Australia*
[c] *Nevis Laboratory, Columbia University, Irvington, NY 10533, USA*
[d] *Smithsonian Astrophysics Observatory, Cambridge, MA 02138, USA*
[e] *University of Adelaide, Adelaide, SA 5005, Australia*
[f] *Enrico Fermi Institute, University of Chicago, Chicago, IL 60637, USA*
[g] *The Adler Planetarium and Astronomy Museum, Astronomy Department, Chicago, IL 60605, USA*
[h] *University of Michigan, Ann Arbor, MI 48109, USA*
[i] *Department of Physics, Columbia University, New York, NY 10027, USA*
[j] *University of Illinois at Champaign-Urbana, Urbana, IL 61801, USA*
[k] *Department of Physics and Astronomy, Louisiana State University, Baton Rouge, LA 70803, USA*
[l] *Department of Physics, Southern University, Baton Rouge, LA 70801, USA*
[m] *Department of Physics, Michigan Technical University, Houghton, MI 49931, USA*

Received 5 August 2000; received in revised form 12 October 2000; accepted 9 November 2000

Abstract

The average extensive air shower longitudinal development profile is measured. Events between 10^{17} and 10^{18} eV recorded by the HiRes/MIA hybrid experiment are used for the average profile. Several functional forms are examined using this average profile. The best-fit parameters for the above functions are determined.

PACS: 96.40.Pq; 98.70.Sa; 13.85.Tp
Keywords: Air shower; Cosmic ray

* Corresponding author.

0927-6505/01/$ - see front matter
PII: S0927-6505(00)00170-5

1. Introduction

The atmospheric nitrogen fluorescence light technique plays an increasingly important role in extremely high energy cosmic ray observations. The success of the Fly's Eye and HiRes [1] experiments encourages the employment of this technique in future projects like the Auger experiment [2], the Telescope Array proposal [3] and space based experiments like EUSO [4] and OWL [5]. In a recent report on the change of cosmic ray composition in the vicinity of 5×10^{17} eV from HiRes/MIA joint data [6], the authors have pointed out that the reconstruction of the shower longitudinal development depends upon the assumed functional form of the features of the shower development. How much do the characteristic parameters of the shower longitudinal development such as the shower maximum and its location, shower rise and shower decay constant depend on which function is employed? In the new technique of shower reconstruction developed for the HiRes monocular data [7], the shower development function plays an even more fundamental role in the shower geometry reconstruction. In effect, the shower geometry is varied until the correct shower width predicted by the average shower function is obtained. The use of an appropriate shower development function is crucial in the determination of shower energy because this is based on the integral of this function. In practice, empirical functions based on data at lower energies or based on theoretical electromagnetic cascade calculation are used at the highest energies, e.g. above 10^{17} eV. However, none of these has been experimentally tested at these energies in the atmosphere. Values of parameters used in trial functions such as the λ in the Gaisser–Hillas (G–H) function [8] and L_0 (for a hadronic shower) in the Greisen function [9] have never been measured in experiments at such a high energy. This is sufficient motivation to carefully test these well-known functions and determine those parameters directly from experimental data. The HiRes/MIA joint experiment meets the necessary conditions for such a high resolution measurement of the shower longitudinal development.

The HiRes prototype detector provides a angular degree by degree measurement of the intensity of the fluorescence light produced by the shower electrons along the shower axis. This light intensity, after corrections, is proportional to the shower development profile. The angular bin signals, however, suffer fluctuations and are contaminated by the direct and scattered Cerenkov light component produced by the same electrons. The source of the fluctuation is sky noise and the statistical fluctuation due to finite sampling of the light. A method to minimize the bin by bin fluctuation is to take averages of the angular bin signals over all the events. This will establish an almost perfect "average shower longitudinal development profile" which can be used to test the various trial functions. In order to do so, however, all showers must be "aligned" and "normalized" so that the showers can be compared with each other in spite of variations of position of shower maximum and shower energy. To carry out the alignment and normalization properly requires that the shower geometry must be well determined. In addition, the Cerenkov components of the signals must be subtracted. Fluorescence light is proportional to the shower size and the proportionality coefficient is geometry related. In the HiRes/MIA joint experiment, the shower geometry is well determined with the help of muon front timing information from MIA, the wide elevation angle range (up to 70°) of the HiRes prototype detector allows for a broad range of shower development to be detected, and the short shower-detector distance (about 3 km) minimizes uncertainties related to the atmospheric attenuation and scattering. We use the same data set selected for the study of the composition of primary cosmic rays [6]. The criteria used to select this sample are well justified there based on a full detector simulation [10].

In the following sections, we will describe the experiment and data set briefly, explain how to minimize the contribution of Cerenkov light and how to subtract the Cerenkov light component in each angular bin, propose a way to normalize the individual showers, and present the average profile and compare it with well-known functions.

2. HiRes/MIA joint experiment and data set

The HiRes prototype was situated at 112° W longitude and 40° N latitude and at a vertical atmospheric depth of 850 g/cm^2. It is [1] composed of 14 optical reflecting telescopes. They image the extensive air shower (EAS) as it progresses through the field of view of the telescope. Nitrogen fluorescence light (300–400 nm) is emitted at an atmospheric depth X in proportion to the number of charged particles in the EAS at that depth. The electrons radiate Cerenkov light in the same band simultaneously. Because of the very forward angular distribution of the Cerenkov light, only those events pointing toward the detector will give rise to signals dominated by Cerenkov light. However, the Cerenkov light can be scattered by molecular and aerosol particles into almost all pixels along the shower track no matter what the shower geometry is. Therefore, the signal recorded by the HiRes detector consists of the sum of fluorescence light, Cerenkov light and various kinds of noise.

The MIA detector is situated about 3.3 km from HiRes and 150 m lower in elevation. It [11] consists of 2500 m^2 of active area distributed in 16 patches of 64 scintillation counters and measures the EAS muon arrival times with a precision of 4 ns and records all hits occurring within 4 μs of the system trigger. Combining such well-determined timing from MIA with the triggered HiRes pixel directions and HiRes timing information allows precise reconstruction of the shower geometry. This is essential in the determination of the atmospheric depth at which the shower passes the triggered HiRes pixels and the optical path length between the shower and the detector.

HiRes/MIA coincident data were collected on clear moonless nights between 23 August, 1993 and 24 August, 1996. The total coincident exposure time was 2878 h corresponding to a duty cycle of 10.9%. 4034 coincident events were observed. For events passing a set of coincidence assurance cuts, the shower trajectory, including arrival direction and core location for each event was obtained in an iterative procedure using the information from both HiRes and MIA [10]. The accuracy of the shower axis determination depends on the number of observed muons, the HiRes angular track length and the core distances from MIA and HiRes. 2491 events are reconstructed via this procedure. Monte Carlo (MC) studies [10] show that the median shower direction error is 0.85° with a median core location error of 45 m.

To insure data quality and maintain good resolution we require that for each event the depth of shower maximum X_m is visible within a minimum observed slant depth interval of 250 g/cm^2, that the track subtends at least 20°, that the accumulated gap between the fired pixels is less than 40% of the total gramage spanned by the shower, that the uncertainty in X_m, ΔX_m, is less than 50 g/cm^2, that the reduced χ^2 for the profile fit not exceed 10 and that the MIA to core distance R_{pMIA} is less than 2000 m. Additionally, we require the minimum viewing angle of the fired tube, θ_h, to be greater than 20° in order to delete events which possess large direct Cerenkov light components. These cuts, as summarized in Table 1, leave a sample of 488 events. The energy distribution peaks at 3×10^{17} and the average Cerenkov light fraction is 15%. There is no event in this sample in which direct Cerenkov light contributes more than 1% of the total signal.

We note that the shower development profile has been fit to the G–H function in order to carry out some of the cuts. However, the use of this function as well as the fit parameters derived from it is for the purpose of event selection only. Hereafter, only the raw data for these selected events is used in the analysis.

Table 1
Event selecting criteria[a]

Variables	Cuts
X_m	$X_l < X_m < X_h$
Track span	$X_h - X_l > 250$ (g/cm^2)
Track angular length	>20°
Total gap in gramage	$<0.4(X_h - X_l)$
ΔX_m	<50 (g/cm^2)
χ^2	<10/DOF
θ_h	>20°
R_{pMIA}	<2 km

[a] $X_h(X_l)$ refers to the depth corresponding to the highest (lowest) bin in the field of view of the detector.

3. Cerenkov light subtraction

HiRes pixel signals are rearranged into a one dimensional series of 1° bins along the shower track by considering the light acceptance of the mirrors according to the geometric position of the shower. As mentioned above, these HiRes bin signals include both fluorescence and Cerenkov light, although the total fraction of direct Cerenkov light is kept low by the imposition of the cuts described above. Bins which correspond to the deeper positions in the atmosphere tend to have more scattered Cerenkov light because the Cerenkov beam accumulates with increasing shower development and the molecular and aerosol scattering gets stronger as the shower penetrates deeper into the atmosphere. The raw signal versus depth, therefore, is not in itself a representation of the shower longitudinal development. We must subtract the scattered Cerenkov light from the observed signal. The resultant corrected signal composed only of the fluorescence light contribution is proportional to the shower size at the corresponding atmospheric depth except for the natural and electronic noise component.

The Cerenkov light produced in an angular bin is calculated by multiplying the average Cerenkov light yield of a single electron with the shower size at the corresponding depth X. The average yield is taken over the energy of shower electrons above the Cerenkov threshold, E_t, and over the emitting angle. The energy spectrum of shower electrons, the angular distribution of Cerenkov light and the pressure dependence of E_t and yield are carefully considered. Details can be found in Ref. [12] and its references.

The contribution of direct Cerenkov light is minimized by the data cuts. The contribution to the bin signal from scattered light from the accumulated Cerenkov beam is estimated as follows: we assume that the Cerenkov light beam in the angular bin is due to shower electrons in the previous adjacent angular bin. After taking into account the attenuation of the Cerenkov light beam traveling through the air between the bins, the contribution of scattered Cerenkov light from the beam into the detector is estimated based on the Rayleigh scattering theory and Mie scattering by aerosol.

The observed signal in this angular bin can then be modified by subtracting the scattered Cerenkov light. The corrected signal can be converted into a shower size for the sake of computing the contribution to the Cerenkov light beam in the next adjacent angular bin. This recurrent procedure requires knowledge of the Cerenkov light beam component in the first angular bin in the field of the view of the detector. If the first signal bin were at the beginning of the shower development, the Cerenkov light component would be zero. The observed signal in this bin would be pure fluorescence which can be converted directly into a shower size. We assume that the first detected bin corresponds to an early enough stage in the shower development so that the zero-Cerenkov-light-component assumption is still approximately true. This subtraction scheme systematically underestimates the Cerenkov fraction in each subsequent bin because the first detected signal from the shower is not at the very beginning of the shower cascade. However, we will find that this systematic error is negligible and the proposed Cerenkov light subtraction is sufficient for our purposes.

4. The normalization of air shower development profile

As mentioned above, all the showers must be aligned in atmospheric depth and be normalized in shower size before one can take the average in bins over events. Most of our events follow a transition curve, namely the shower size increases rapidly as it develops in the atmosphere until reaches its maximum, N_m, then it starts decreasing because shower electrons begin to lose more energy by ionization than by radiation of high energy gammas. The maximum size of a shower is approximately proportional to the energy of the primary particle. After subtracting the Cerenkov light components, the signals are converted into shower sizes by taking the geometry and atmosphere related light collecting efficiency and attenuation effect into account. The showers are normalized with respect to energy by their maximum size, i.e. $N(X)/N_m$, denoted as $n(X)$. All the shower sizes are normalized to one as they reach their maxima.

Air shower development fluctuates in atmospheric depth due to fluctuations in the hadronic multiparticle production (which depends on the nature of the primary nucleus) and electromagnetic processes. As a consequence, the position of the shower maximum, X_m, varies from event to event. One can express the shower longitudinal development as a function of the shower "age", defined as $s = 3X/(X + 2X_m)$, instead of depth, X. By using s, the shower longitudinal development is universally described as a rising phase from 0 (initial position of the shower) to 1 (shower maximum) and the decay phase from 1 to 3 (infinite depth). The physical shower has an effective extent from 0 to 2, however.

After the Cerenkov light subtraction, the observed signal profiles of individual events span a range of atmospheric depth and show the shower maximum through their convex shape. The best way to find the position of shower maximum in the presence of statistical fluctuations is to carry out a local fit with a rather general function. We use a parabolic function to fit the data in order to determine both the location and the size of the shower maximum. The only constraint to this function is that it must be convex. Here, "local fitting" means that the fitting procedure is only applied to those data points near the maximum to minimize the bias in the location of the maximum caused by using such a symmetric trial function. The method can be iterated to remove points far from the maximum. We find that the iteration affects the location of shower maximum by less than 4% however and we do not use it in what follows.

With shower maximum and size at maximum determined, the showers are normalized in size and aligned in depth. Fig. 1 shows all 488 showers plotted with normalized shower size, n, versus shower age, s. In order to more easily see the change of the density of the dots in the scatter plot, we let each entry represent three measurements. 6069 entries in total out of 18 230 bins signals are picked randomly and plotted. We note that there is a 20% fluctuation in n near the shower maximum. The distribution of n at shower maximum is shown in Fig. 2. The residuals in n, defined as the ratio between the deviation from the expectation value and the error associated with the individual bin signal, are well distributed as a Gaussian centered at 0 with a width of 0.94. The main sources of this

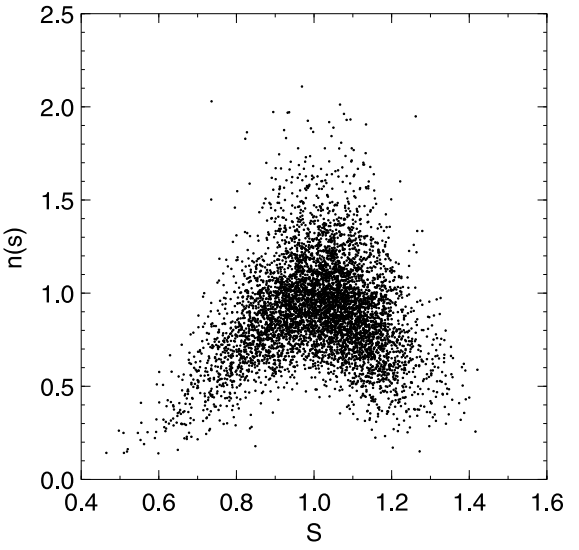

Fig. 1. Aligned shower longitudinal development. Only one-third of the data is shown for clarity. Each point represents the fluorescence light signal in a 1° bin in an event. The events are normalized to 1 at individual shower maximum via a local parabolic fit.

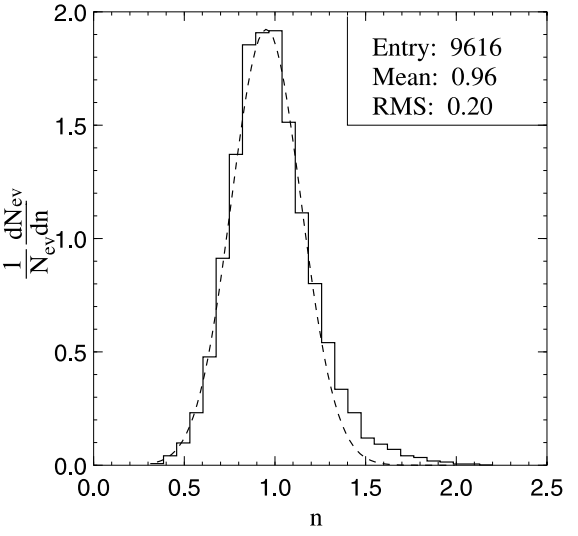

Fig. 2. The fluctuation of normalized fluorescence light signals around shower maximum, $0.9 < s < 1.1$. The dashed line represents a Gaussian fit, see the text for the details.

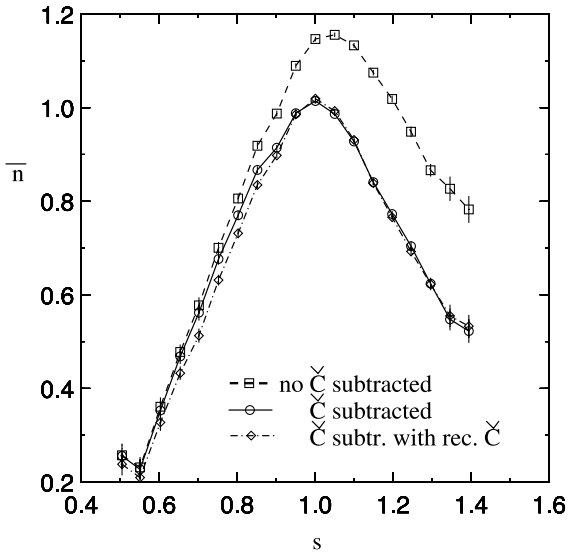

Fig. 3. The average shower transition curve. Solid line plus circles refers to the bin signal based recurrent Cerenkov-light-subtracting method, the dashed line plus squares is the raw signal including the Cerenkov light. The dash-dotted line plus diamonds corresponds to a different Cerenkov light subtraction method (see the discussion on systematic error in Section 6). Lines are drawn to guide the eye.

fluctuation are sky noise, statistical fluctuation, the error in shower geometry determination, the error in Cerenkov light subtraction and the error in determining shower maximum. The first three, and particularly the first one, contribute more than 80% to the total fluctuation in the signal. The error from Cerenkov subtraction contributes the least.

The data is binned into age intervals, instead of the original angular bin. We take an average of the normalized shower size within each bin over all events to obtain an average shower development profile. The curve is well determined between $s = 0.5$ and 1.25. We demonstrate the effect of the Cerenkov light subtraction in Fig. 3, by plotting the average shower transition curves before and after the subtraction in the same plot.

5. Tests of trial functions

After calculating the average normalized shower longitudinal development profile, we fit the shape of the profile with several well-known trial functions such as the G–H [8], Greisen [9] and Gaussian forms.

In order to describe the characteristics of the shower longitudinal development, i.e. the asymmetric rising–falling shape, Gaisser and Hillas introduced a function which depends on the essential characteristics of air shower: the initial point, X_0, the shower maximum, N_m, the shower maximum location, X_m, and the shower decay length, λ. Except for N_m which is in number of shower electrons, all the parameters are in units of atmospheric depth, g/cm^2. The function describes the change of the shower size with the atmospheric depth as

$$N(X) = N_m \left(\frac{X - X_0}{X_m - X_0} \right)^{(X_m - X_0)/\lambda} e^{(X_m - X)/\lambda}, \quad (1)$$

where the atmospheric depth, X, is in g/cm^2.

Translating the depth X into age s and using the normalized shower size $n = N/N_m$, Eq. (1) becomes

$$n(s) = \left(1 - \frac{1-s}{3-s} \frac{3T_m}{T_m - T_0} \right)^{T_m - T_0} e^{3T_m(1-s)/(3-s)}, \quad (2)$$

where $T_m = X_m/\lambda$ and $T_0 = X_0/\lambda$ are the two remaining parameters. Parameter T_0 is constrained to be less than $(2s_{min}/(3 - s_{min}))T_m$, where s_{min} is the lower limit of the data points (about 0.5 as shown in Fig. 3). The comparison of this function with the data is shown in Fig. 4. The two parameters are strongly correlated.

The fit is poor at small and large s, particularly beyond $s = 1.3$. While a possible reason for the deviation of those 3–4 points may be poor statistics, a detailed systematic error analysis is described in Section 6.

The second trial function is the Greisen function which was suggested [9] to describe the development of a pure electromagnetic shower. Depth is therefore expressed in the unit of radiation length, $L_0 = 36.66$ g/cm^2. The function is defined by a single parameter, $y = X_m/L_0$, and has a form

$$N(T) = \frac{0.31}{\sqrt{y}} e^{T\left(1 - \frac{3}{2}\ln s\right)}, \quad (3)$$

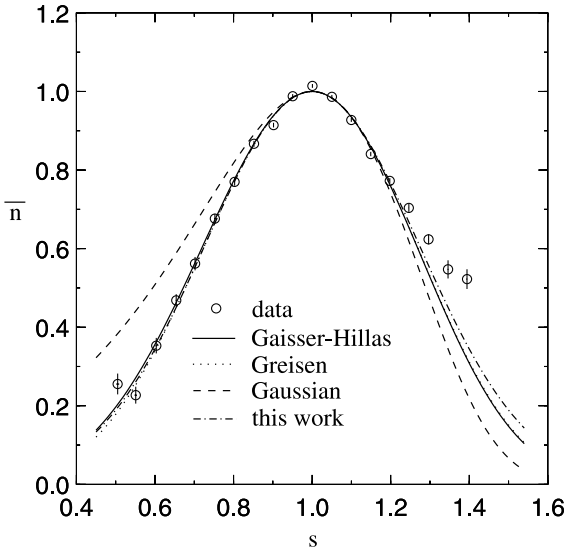

Fig. 4. Comparison between the data and test functions. Circles refer to data. The solid line refers to the G–H function, the dotted line to the Greisen function, the dashed line to the Gaussian function and the dash-dotted line to the newly proposed symmetrical Gaussian function of the shower age.

where $T = X/L_0$ refers to the atmospheric depth in radiation lengths in the air. Since the age s appears explicitly in the formula, it is straightforward to rewrite it as a function of either s or T. It is apparent after conversion to a function of s that the radiation length no longer appears explicitly in the formula. This feature of the Greisen function make it potentially useful for the description of a hadronic shower with a single parameter y. However, the meaning of L_0 need to be changed. In the case of electromagnetic cascade, Greisen shows that $y = \ln(E_0/E_c)$ fits a elongation law with a rate about 80 g/cm^2 where the E_c refers to the electron critical energy. We will see how the rate is changed to fit the case of hadronic shower below. The fit of the Greisen function to our measured average shower is shown in the dotted line in Fig. 4.

In the Fly's Eye data analysis [13], the poorer detector resolution dominated over the shape of the shower longitudinal development, and a symmetric Gaussian in X could be used to represent the shower longitudinal development. Using $\xi = \sigma/X_m$ as the single parameter, the Gaussian can be normalized by following the rule set in previous sections, i.e.

$$n(s) = \exp\left\{ -\frac{1}{2\xi^2}\left(\frac{1-s}{1-s/3}\right)^2 \right\}. \quad (4)$$

The result is also plotted in Fig. 4. It is a poor fit to the data with a $\chi^2 = 26$ per degree of freedom. Thanks to the significantly improved resolution, this experiment provides the first clear observation of an asymmetrical air shower development profile in X at 10^{17}–10^{18} eV.

However, based on the result of this experiment, we observe that the average longitudinal development profile of air showers appears quite symmetrical as a function of shower age, s. A simple symmetrical Gaussian shaped function of age can be used to describe shower profiles. Since the function is centered at 1, it is governed by only one parameter, i.e. the width of the function, denoted as σ. This fit is shown in Fig. 4 also. Hereafter, we call this function the "new Gaussian function" to distinguish it from the one that is symmetric in the depth variable.

We plot the fit results in the form of deviations in Fig. 5. Quantitatively, the χ^2 per degree of freedom for G–H, Greisen and the "new Gaussian function" are 1.93, 1.87 and 1.79 respectively. They all have essentially the same goodness of fit. More data beyond the region currently covered is required to further differentiate between them. From a practical standpoint however, the G–H function contains too many parameters, especially X_0 which is not directly measured in experiments and is consequently poorly defined. These parameters are strongly correlated. The Greisen function does not have this problem because it fits the data with a single parameter. Both functions need a scale to measure the shower development, however. The scale is given by λ and L_0, respectively. The scale must be associated with the type of primary particle. This actually reduces the freedom of fitting in the reconstruction of real experimental events. One has to set the scale as a parameter in a complete fitting procedure. The "new function" proposed in this work is more practically useful in real shower reconstruction. As a function of depth, it has the form

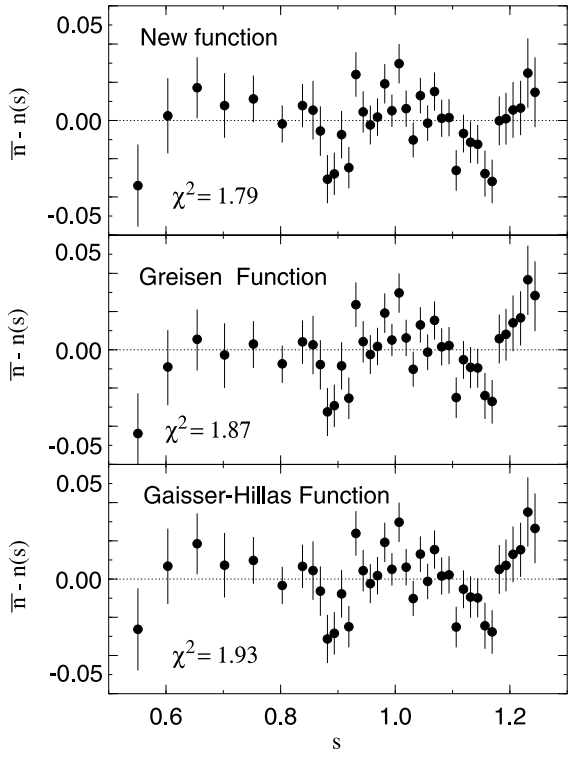

Fig. 5. Deviation of the data from the fits. The χ^2 is per degree of freedom.

$$n(X) = \exp\left\{ -\frac{2}{\sigma^2}\left(\frac{X - X_m}{X + 2X_m}\right)^2 \right\}. \quad (5)$$

This function uses a single parameter, X_m, to locate a shower in the atmosphere, and a single parameter, σ, to indicate the shower width and it is *scale-free*. The last feature is very useful since the composition is a-priori unknown.

6. Systematic error analysis

In order to investigate the reasons for deviation from the test functions at both early and late stages of shower development, we apply the above analysis to MC simulated events. The generator used here is the full simulation code of the HiRes/MIA detector developed in the composition study [6]. It is driven by a shower generator based on the CORSIKA package [14]. It produces the shower size using the G–H function with full fluctuations in X_m, N_m, X_0 and λ. The fluctuation in muon density and muon arrival time on the ground is generated according to parameterizations of CORSIKA simulated events. All details of the detector are carefully considered including the sky noise, atmospheric attenuation, "ray-tracing", phototube response, electronics and triggering. Generated data are passed through the complete calibration and reconstruction procedure just like the real data. The details of the generator and the comparison with the data can be found in Ref. [10]. Fig. 6 shows that the overall quality of the fit is good. This means that the Cerenkov subtracting scheme, shower maximum finding and normalization procedure proposed in this paper work well. The shower longitudinal development function is reconstructed almost exactly except for the few points at the beginning and the end of the shower

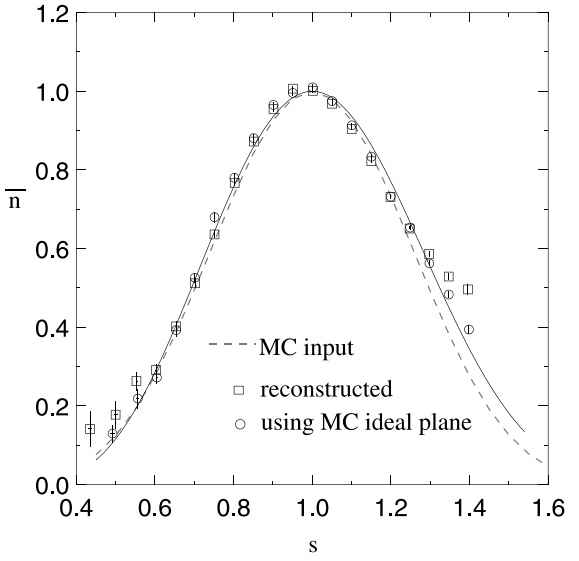

Fig. 6. The average longitudinal profile of MC generated showers. Open squares represent the results from the standard shower reconstruction; the open circles represent the same analysis but with the shower-detector plane direction used correcting the tube signal replaced with the ideal input parameters. The dashed lines represents the average input shower profile. It is broadened by the shower reconstruction and event selection about 9 g/cm^2.

as is the case for the real data. The deviation turns out to be associated with the correction to tube signals which lie far from the shower-detector plane. Details of this correction can be found in Ref. [10]. Briefly, a tube can be triggered even if it is not located exactly on the shower-detector plane since the shower has a finite lateral width, the mirror image on the focal plane has a finite spot size and the broadening effect due to the atmospheric scattering. The amount of light reaching the detector can be calculated by correcting the amount of measured light with a response function in the off-plane angle. This function is determined by performing a careful "ray-tracing" procedure which folds all of the effects in. It turns out to be a Gaussian with a typical width of a few tenths of a degree depending on the shower distance and the shower age. On the other hand, we know that there is an uncertainty in the determination of the shower-detector plane direction of about 0.7° [10]. This uncertainty causes a systematic overcorrection in the signals for off plane tubes. This becomes worse for a tube located far from the center of the phototube cluster. This effect can be verified by simply substituting the ideal MC input shower-detector plane for calculating the correction and comparing with the correction using the fitted shower-detector plane. This is shown in Fig. 6. The effect on the beginning and end of the average profile is clear.

One way to handle this systematic error would be to correct it based on this MC simulation result. Another approach is to simply drop those affected points in the fitting procedures. We prefer the latter for several reasons. First, it avoids introducing any modeling dependence. Secondly, the points being dropped at age >1.25, correspond to positions deeper than $1.43X_{\rm m}$, or about 860 g/cm^2 in the atmosphere, where the uncertainty in atmospheric attenuation is greatest. As a part of the systematic uncertainty study, we varied the atmospheric parameters [6] by one standard deviation from their most probable values in the shower reconstruction. We observed that there is no effect for most of the average profile and that this variation affected only the last few deepest points. This effect is smaller than that produced by the shower-detector plane error. Finally, in practice, dropping those points does not change our result because of the relatively large statistical errors associated with those points.

We now discuss the systematic error caused by setting the Cerenkov light to be zero in the first angular bin in the field of view of the detector. Based on the previous results, we know that the G–H function works well in describing the shower longitudinal development. We can use the G–H function in a least χ-square fitting procedure event by event. Since in this case we know the shape of the shower, the Cerenkov light component in all angular bins can be calculated. The fraction of Cerenkov light in each bin is compared to our original method in Fig. 7. It is clear that most of the Cerenkov light is subtracted with our bin signal based Cerenkov light subtracting scheme. Only 7.7% of the Cerenkov light is systematically underestimated. This is a minor effect in calculating the average transition curves as shown in the Fig. 3. The diamonds in the figure are obtained by carrying out the same averaging and normalization procedure as before but with the Cerenkov light fraction in each bin replaced by that determined

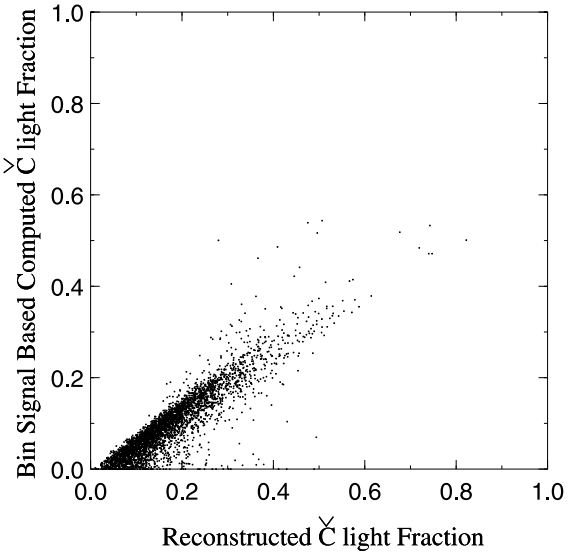

Fig. 7. Comparison of Cerenkov light fraction in each 1° bin. The x-axis is the reconstructed Cerenkov light fraction using G–H function and the y-axis is the fraction from the bin by bin recurrent Cerenkov-light-subtracting scheme.

using the G–H function. The points are visibly lower which makes the profile appear slightly wider. However, the widening is not large enough to change our conclusion on the shape of the longitudinal development function. For instance, the values of fitted parameter T_0 and T_m are -2.57 and 8.6, respectively, which are consistent with the result listed below.

The other systematic issue is the reliability of our maximum searching by using local fitting with a parabolic function. The uncertainty associated with this method is demonstrated by comparing the maxima with those obtained from the reconstruction procedure using the G–H profile. Fig. 8(a) shows the comparison between the X_m's and Fig. 8(b) shows the difference between the N_m's. The other way to illustrate the uncertainty is to compare the resolution functions in X_m and N_m from simulation for both methods. It turns out the resolution in X_m for local parabolic fitting is 16% worse than the standard G–H approach, and the resolution in N_m is comparable in both cases.

We also study whether or not the shape of the average profile is biased by the shower reconstruction and event selection. The generated showers are used since their "true" shape are known. This allows us to compare the average profile before and after the event survives the trigger, reconstruction and event selection. A slight broadening of the average profile is observed and demonstrated in Fig. 6 (from dashed line to the solid line). The broadening is about 9 g/cm^2 in terms of the λ parameter in the G–H function. This effect is less than the experimental error.

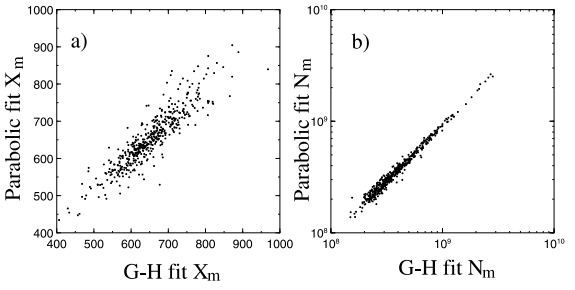

Fig. 8. Comparison of shower maxima for reconstruction with the G–H function and with local parabolic fitting. (a) for X_m's and (b) for N_m's.

7. Results and conclusion

In order to extract the best values for the parameters, T_m, T_0, y and σ, in the G–H, Greisen and the "new Gaussian function", a well-reconstructed data set is used. The parameters are determined to be

$$T_m = 9.7 \pm 2.0, \tag{6}$$

$$T_0 = -3.2 \pm 2.9, \tag{7}$$

$$y = 11.11 \pm 0.34, \tag{8}$$

$$\sigma = 0.272 \pm 0.002. \tag{9}$$

A strong correlation between T_m and T_0 is found for the G–H function. This correlation can be expressed as $T_0 \sim -0.10T_m^2 + 0.74T_m - 0.10$ and is shown in Fig. 9.

These results imply: (1) the strong correlation between parameters in the G–H function means that the data can be fit with a simpler form. Alternatively one can fix one of those parameters and apply the correlation between them in the shower reconstruction; (2) the parameter λ in the G–H

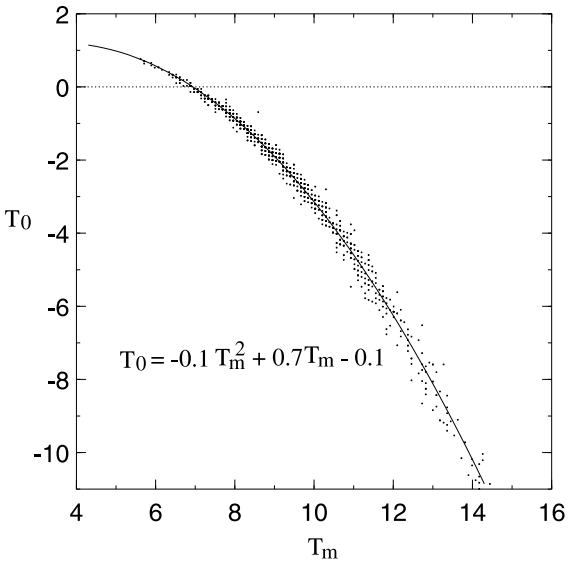

Fig. 9. The correlation between the parameter T_m and T_0 in G–H function (2).

function can be estimated to be 67 ± 11 g/cm^2 by using the average $X_{\max} = 651.9 \pm 3.5$ g/cm^2; (3) the parameter T_0, or X_0, is likely to be a negative number in any individual shower fit. It is thus difficult to interpret as the first interaction point of a shower; (4) the parameter y, defined as X_m/L_0 in the Greisen function, is close to T_m, defined as X_m/λ. This implies that the best value of the parameter L_0, 58.7 ± 2.0 g/cm^2, is no longer the radiation length. This is to be expected since it is used to describe a hadronic shower; (5) a symmetrical function in age is a suitable representation of the shower longitudinal profile. This function is depth-scale invariant.

In summary, the shape of the EAS longitudinal development is investigated in the energy range from 10^{17} to 10^{18} eV with the HiRes/MIA hybrid experiment. The profile is quite symmetrical as a function of the age of the shower. The "new Gaussian function" (5), the Greisen function (3) and the G–H function (2) describe the shower shape almost equally well, with the χ^2's of the test 1.79, 1.87 and 1.93 respectively. This is the first direct measurement of the shower average longitudinal development profile at these energies and covering such a wide range of shower age.

Acknowledgements

We acknowledge the assistance of the command and staff of Dugway Proving Ground. We are very grateful for discussions with James W. Cronin and Paul Sommers. This work is supported by the National Science Foundation under contract no. PHY-93-21949, PHY-93-22298 and the US Department of Energy.

References

[1] T. Abu-Zayyad, et al., The prototype high resolution fly's eye cosmic ray detector, Nucl. Instrum. Meth. A, in press.
[2] A. Etchegoyen, et al., The Auger Collaboration, Pierre Auger Project Design Report, second ed., November 1996.
[3] The TA collaboration, in: M. Fukushima (Ed.), Telescope Array Design Report, 2000. http://www-ta.icrr.u-tokyo.ac.jp/TA Proposal.
[4] L. Scarsi, et al., EUSO Collaboration, in: L. Scarsi (Ed.), Extreme Universe Space Observatory, A Proposal for the ESA F2/F3 Flexible Missions, IFCAI/CNR, Via Uga La Malfa 153, 90146 Palermo, Italy, 2000.
[5] O. Catalano, in: D. Kieda, et al. (Eds.), Proceedings of the 26th International Conference (ICRC), vol. 2, University of Utah, Salt Lake City, Utah, 1999, p. 411.
[6] T. Abu-Zayyad, et al., Phys. Rev. Lett. 84 (2000) 4276.
[7] T. Abu-Zayyad, et al., in: D. Kieda, et al. (Eds.), Proceedings of the 26th International Conference (ICRC), vol. 3, University of Utah, Salt Lake City, Utah, 1999, p. 264.
[8] T. Gaisser, A.M. Hillas, Proc. 15th ICRC, vol. 8, Plovdiv, 1977, p. 353.
[9] K. Greisen, Annu. Rev. Nucl. Sci. 10 (1960) 63.
[10] T. Abu-Zayyad, et al., Measurement of the Cosmic ray flux and composition from 10^{17} to $10^{18.3}$ eV using a hybrid fluorescence technique, Astrophys. J., submitted for publication.
[11] A. Borione, et al., Nucl. Instrum. Meth. A 346 (1994) 329.
[12] R.M. Baltrusaitis, et al., Nucl. Instrum. Meth. A 240 (1985) 410.
[13] D.J. Bird, et al., Phys. Rev. Lett. 71 (1993) 3401.
[14] D. Heck, et al., Preprint: Institut fur Kernphys., University of Karlsruhe, FZKA-6019, Kernforschungszentrum, Karlsruhe, February 1998.